Available online at www.sciencedirect.com
ScienceDirect
International Journal of Heat and Mass Transfer 51 (2008) 1542–1550
International Journal of HEAT and MASS TRANSFER
www.elsevier.com/locate/ijhmt

Heat transfer in the evaporator section of moderate-speed rotating heat pipes

F. Song, D. Ewing, C.Y. Ching *

Department of Mechanical Engineering, McMaster University, Hamilton, Ontario, Canada L8S 4L7

Received 29 September 2006; received in revised form 25 April 2007
Available online 7 September 2007

Abstract

Experiments were performed to investigate the heat transfer mechanism in the evaporator section of non-stepped rotating heat pipes at moderate rotational speeds of 2000–4000 rpm or accelerations of 40*g*–180*g*, and evaporator heat fluxes up to 100 kW/m^2. The thermal resistance of the evaporator section as well as that of the condenser section was examined by measuring the axial temperature distributions of the flow in the core region of the heat pipe and along the wall of the heat pipe. The experimental results indicated that natural convection heat transfer occurred in the liquid layer of the evaporator section under these conditions. The heat transfer measurements were in reasonable agreement with the predictions from an existing rotating heat pipe model that took into account the effect of natural convection in the evaporator section.

Keywords: Rotating heat pipe; Evaporator heat transfer; Natural convection

1. Introduction

Wickless rotating heat pipes are highly effective two-phase heat transfer devices that have been proposed and used for thermal management in rotating machinery [1–3]. The liquid flow and heat transfer in rotating heat pipes depend on a number of factors, including the heat pipe design, the working fluid and fluid loading, the rotational speed or centrifugal acceleration, and the heat flux. The liquid condensate in rotating heat pipes is usually fully annular along the inner surface when the heat pipes operate at moderate rotational speeds with accelerations greater than approximately 40*g* of interest here [4]. Models have been developed for the overall heat transfer performance of rotating heat pipes by solving the governing equations for the flow and heat transfer of the liquid annulus throughout the heat pipe [5–8]. A modified Nusselt-type laminar film condensation model has been found to be applicable for predicting the heat transfer in the condenser section [9,10]. The heat transfer in the evaporator section, however, remains less well understood.

The heat transfer mechanism in the evaporator section of stepped rotating heat pipes, where the liquid film thickness is usually more than 1 mm, appears to be similar to pool boiling under acceleration [5,10]. Natural convection and nucleate boiling occurred in sequence as the heat flux increased, with the onset of nucleate boiling being suppressed to higher heat fluxes with rotational speed. Once nucleate boiling was initiated, the thermal resistance of the liquid film in the evaporator was normally small compared to that in the condenser [11], and thus could be neglected while considering the overall heat transfer performance of rotating heat pipes. Somewhat surprisingly, these measurements suggested the evaporator heat transfer in the natural convection region was independent of rotational speed [5], which was not observed for natural convection in liquid pools under acceleration.

The liquid film thickness in the evaporator section of non-stepped rotating heat pipes is usually much smaller than in stepped heat pipes and is often comparable to or

* Corresponding author. Tel.: +1 905 525 9140x24998; fax: +1 905 572 7944.
E-mail address: chingcy@mcmaster.ca (C.Y. Ching).

0017-9310/$ - see front matter © 2007 Elsevier Ltd. All rights reserved.
doi:10.1016/j.ijheatmasstransfer.2007.07.020

Nomenclature

a	centrifugal acceleration [m s^{-2}]
A	cross-section area [m^2]
c_p	specific heat at constant pressure [J kg^{-1} K^{-1}]
g	gravitational acceleration [m s^{-2}]
h_{fg}	latent heat of phase transformation [J kg^{-1}]
L	length [m]
$\dot{m}_c$	mass flow rate of the cooling water in the condenser water jacket [kg s^{-1}]
m_g	mass of non-condensable gas [kg]
Nu_δ	liquid film Nusselt number, $\frac{h\delta}{k_l}$
p	vapour pressure corresponding to saturation temperature [Pa]
Q	heat transfer rate [W]
r	local radius [m]
R	thermal resistance [K/W]
Ra_δ	liquid film Rayleigh number, $\frac{\rho_l\omega^2 r\cos\alpha\beta\Delta T\delta^3}{\mu_l\alpha_l}$
Ra^*_δ	modified liquid film Rayleigh number, $\frac{\rho_l\omega^2 r\cos\alpha\beta\Delta T\delta^3}{\mu_l\alpha_l}\left(1+\frac{h_{hg}\dot{V}\delta}{c_{p_l}\alpha_l\Delta T}\right)$
R_g	gas constant [J kg^{-1} K^{-1}]
T	temperature [°C]
$\dot{V}$	volumetric evaporation rate per unit area [m s^{-1}]
α	taper angle [°], or thermal diffusivity [m^2 s^{-1}]
β	thermal expansion coefficient [K^{-1}]
δ	liquid film thickness [m]
μ	dynamic viscosity [kg m^{-1} s^{-1}]
ρ	density [kg m^{-3}]
ω	Angular velocity [rad s^{-1}]

Subscripts

a	adiabatic section
ac	active portion of the condenser
c	condenser section
e	evaporator section
g	non-condensable gases
i	inner wall or inlet of water jacket
in	inactive portion of the condenser
l	liquid
o	outer wall or outlet of water jacket
v	vapour core
w	wall

smaller than the diameter of typical vapour bubbles (0.1–1 mm) [12]. In this case, it was thought film evaporation would occur rather than nucleate boiling [11,13], and the heat transfer has been modeled as such in previous models for non-stepped heat pipes [6–8]. The initial models assumed conduction across the liquid film in the evaporator [6,7], while a recent model [8] considered the effect of acceleration-induced natural convection within the thin liquid film using a correlation developed for natural convection in liquid pools in a rotating boiler [14]. It was found that predictions from the model that considered natural convection were in much better agreement with measurements of the overall performance of non-stepped heat pipes at moderate rotational speeds ($40 < a/g < 180$) than those that only considered conduction [15]. Heretofore, however, there does not appear to have been measurements on non-stepped heat pipes that could be used to directly determine the heat transfer coefficient, or the thermal resistance of the evaporator section at moderate rotational speeds.

The objective of this study was to examine the heat transfer mechanism in the evaporator section of non-stepped rotating heat pipes at moderate rotational speeds. The experiments were performed for two heat pipes, one with an inner tapered condenser and the other with a cylindrical inner surface. The temperature distributions along the wall and the core regions of the heat pipes were measured using thermistors embedded in the heat pipes. The experimental facility and the heat pipes tested are described in the next section, followed by the experimental results and comparison to predictions from the models for the performance of rotating heat pipes.

2. Experimental methodology

The rotating heat pipes were tested using the facility shown in Fig. 1, also used in Song et al. [15]. The heat pipe was fit inside a Teflon sleeve that was then pressed into a stainless steel tube supported by two self-aligning bearings, and driven by a motor capable of rotational speeds up to 4775 rpm. One end of the heat pipe was heated using a dedicated induction heating unit that had a 125 mm long heating coil. The total length of the hollow working section in the heat pipes encased by the induction coil (the evaporator section) was approximately 114 mm. The end cap at the evaporator end was a 3 mm thick copper assembly that was also positioned within the induction coil during the experiments. The induction heating unit could supply heat fluxes up to approximately 100 kW/m^2 into the evaporator section. The heat transfer through the heat pipe was removed from the other end by flowing cooling water through a plastic jacket that encased the condenser. The length of the condenser section that was cooled by the flowing water in the jacket was 98 mm. The water flow to the jacket was provided using a closed loop system. The inlet water temperature was maintained constant during the tests using a PID controlled tape heater wrapped on the pipe leading to the water jacket. The volumetric flow rate of the water was measured using a rotameter with an uncertainty of ±1 mL/s, while the inlet and outlet water temperatures were measured using T-type thermocouples at the entrance and exit of the water jacket. The rotameter was calibrated by measuring the total flow over a given period of time. The thermocouples were calibrated using a

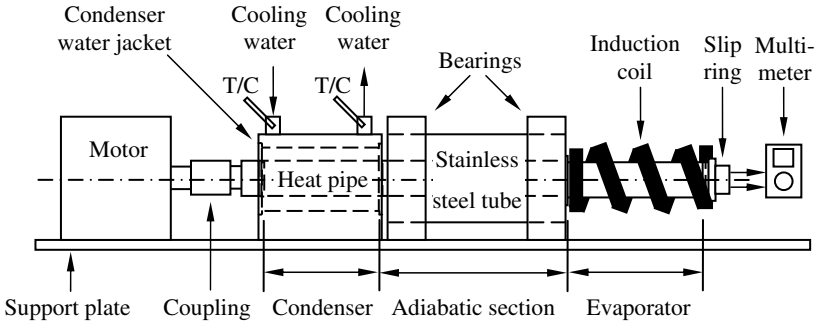

Fig. 1. Schematic of the rotating heat pipe test facility with induction heating at the evaporator and a cooling jacket at the condenser.

RTD thermometer with an uncertainty of ±0.025 °C. It was found that the temperature measurements from these two devices were within ±0.3 °C over the temperature range of interest here [15].

The heat transfer through the heat pipe, Q, was determined by applying an energy balance at the condenser water jacket given by

$$Q = \dot{m}_c c_p (T_{c,o} - T_{c,i}) = \dot{m}_c c_p \Delta T_c \quad (1)$$

where $T_{c,i}$ and $T_{c,o}$ are the inlet and outlet water temperature. The relative uncertainty in the heat transfer measurements (dQ/Q) was determined following the approach of Coleman and Steele [16]. The 95% confidence intervals for heat transfer rates above 0.6 kW was less than approximately ±8%, while it was up to ±20% for lower heat transfer rates (0.2 kW).

The experiments were performed for two copper wickless heat pipes with distilled water as the working fluid. Both heat pipes had cylindrical adiabatic and evaporator sections. One heat pipe had a 2°-tapered condenser section, while the other had a cylindrical condenser as specified in Table 1. The tapered heat pipe was filled with 9.2 g of water, while the cylindrical heat pipe was filled with 6.3 g of water. The fluid loadings were determined based on predictions from the rotating heat pipe model of Song et al. [8]. For the cylindrical heat pipe, the model predictions showed that 6.3 g was the minimum fluid loading to prevent dry out for the current test conditions. The 9.2 g of water in the tapered heat pipe yielded an average liquid film thickness in the evaporator that was approximately twice that in the cylindrical heat pipe with 6.3 g of water, thus allowing the examination of the heat transfer in the evaporator section for different liquid layer thicknesses. The axial temperature distributions along the heat pipe wall were measured using four miniature thermistors embedded in

Table 1
Specifications of the test rotating heat pipes and test conditions

	Tapered heat pipe	Cylindrical heat pipe
Overall length	400 mm	400 mm
Length of cylindrical sections	298 mm	400 mm
Length of tapered section	102 mm	0 mm
Evaporator taper	0°	0°
Adiabatic taper	0°	0°
Condenser taper	2°	0°
Heat pipe wall material	Copper	Copper
Heat pipe outer diameter	25.4 mm	25.4 mm
Wall thickness @ Condenser end cap	6.4 mm	3.2 mm
Wall thickness @ Evaporator end cap	2.8 mm	3.2 mm
Working fluid	Distilled water	Distilled water
Working fluid loading	9.2 g	6.3 g
Heat input to the evaporator	0.2–0.7 kW	0.2–0.7 kW
Heat flux at the evaporator section	30–100 kW/m^2	30–100 kW/m^2
Rotational speed	2000–4000 rpm	2000–4000 rpm
Centrifugal acceleration	40g–180g	40g–180g
Cooling water inlet temperature at the plastic jacket surrounding the condenser	20 °C	20 °C

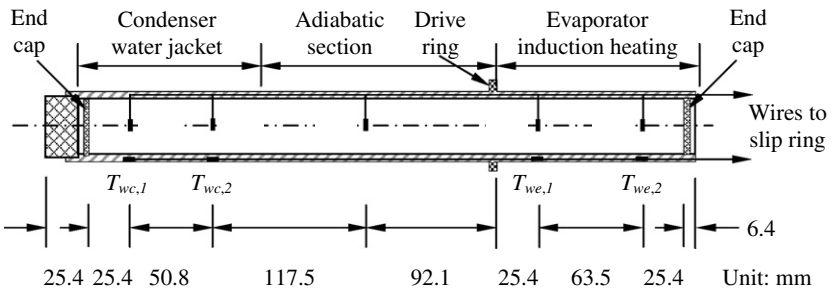

Fig. 2. Schematic showing the locations of the thermistors embedded in the heat pipe wall and core region.

the wall, while the temperature distributions of the flow in the core region were measured using five thermistors embedded through the wall into the center of the core at the positions shown in Fig. 2. The thermistor wires were connected to the rotor terminals of a high-speed slip ring that was mounted onto the evaporator end of the heat pipe. The resistance outputs of the thermistors were measured on the stator side of the slip ring using a multimeter. The contact resistance of the slip ring during operation was on the order of $10^{-3}\,\Omega$, which was much smaller than the resistance outputs of the thermistors that were typically 10^{3}–$10^{5}\,\Omega$. The thermistors were calibrated prior to being installed in the heat pipes using the RTD thermometer with the uncertainty of ±0.025 °C similar to the thermocouples above, yielding a calibration with an uncertainty of approximately ±0.25 °C for the temperature range of interest here.

Non-intrusive measurements of the wall temperature distribution were also performed independently using a thermal imaging camera as has been done in previous investigations [5,15]. The camera had a resolution of approximately 0.55 mm and an accuracy of ±1 °C in the temperature range 0–100 °C and ±1% of the actual readings for temperatures above 100 °C [15]. The measurements suggested that the average of the wall temperatures measured at the two points in the evaporator section ($T_{we,1}$ and $T_{we,2}$ in Fig. 2) with the thermistors were representative of the wall temperature of the evaporator section. The condenser section was encased by the cooling water jacket so the wall temperature distribution in that section could not be measured using the thermal imaging camera.

3. Experimental results and discussion

Typical temperature distributions along the wall and the core regions of the two heat pipes measured with the thermistors at rotational speeds of 2000 and 4000 rpm are shown in Figs. 3 and 4. The test data at 3000 rpm were found to fall between the data at 2000 rpm and 4000 rpm with similar trends, and are not included here for clarity. The temperature of the wall decreased from the evaporator section to the condenser section for both heat pipes, with the temperature drop along the wall in each section being up to 20% of that between the ends of the heat pipes. Additional measurements using the thermal imaging camera showed the temperature at the outer surface of the evaporator end cap was up to 15 °C higher than that of the evaporator wall near the end cap. This was most likely due to the heating of the copper end cap by the induction heating unit. Much of this heating would be conducted to the evaporator wall where it could be transferred to the adjacent liquid annulus, contributing to the temperature drop along the wall in the evaporator. The wall temperature drop in the condenser was comparable to that in the evaporator.

The temperature measured in the core region of both heat pipes was not uniform as was expected. For example, the change along the tapered heat pipe was as large as

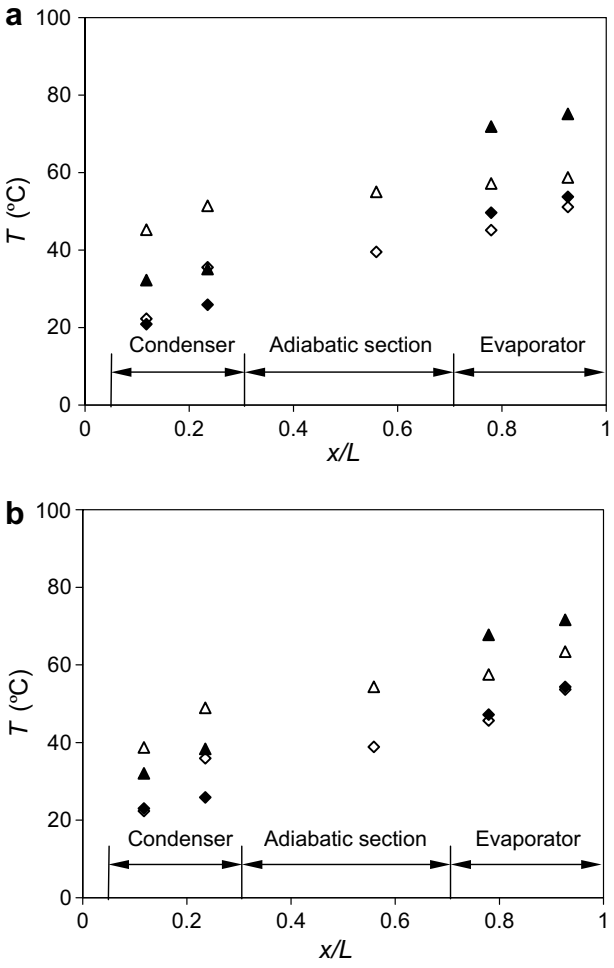

Fig. 3. Typical axial temperature distributions in the wall (solid symbols) and the core region (open symbols) of the tapered heat pipe at (a) 2000 rpm, and ◆◇ 0.30 kW, ▲△ 0.68 kW; and at (b) 4000 rpm, and ◆◇ 0.38 kW, ▲△ 0.69 kW.

30 °C. The estimate of the pressure drop in the vapour flow due to friction and momentum change from vapour condensation [10,17] was typically on the order of 10 Pa that would cause a negligible change in the local saturation temperature. The heating or cooling of the thermistor sensors in the evaporator and condenser sections due to conduction from or to the heat pipe wall was estimated to be approximately 1 °C for the highest heat flux of 100 kW/m^2. The flow in the core region could be a liquid–vapour mixture rather than pure vapour flow that could contribute to the measurement errors, but none of these effects appeared to be consistent with the result that the temperature change in the core region increased with rotational speed and decreased with heat flux. The temperature change in the core region of the evaporator section occurred in both heat pipes and was thought to be due to the flow near the end cap of the evaporator section being superheated due to the interaction with the end cap that was considerably hotter than the evaporator wall. This interaction could be complicated by the presence of a flow reversal in the vapour flow near the evaporator end as

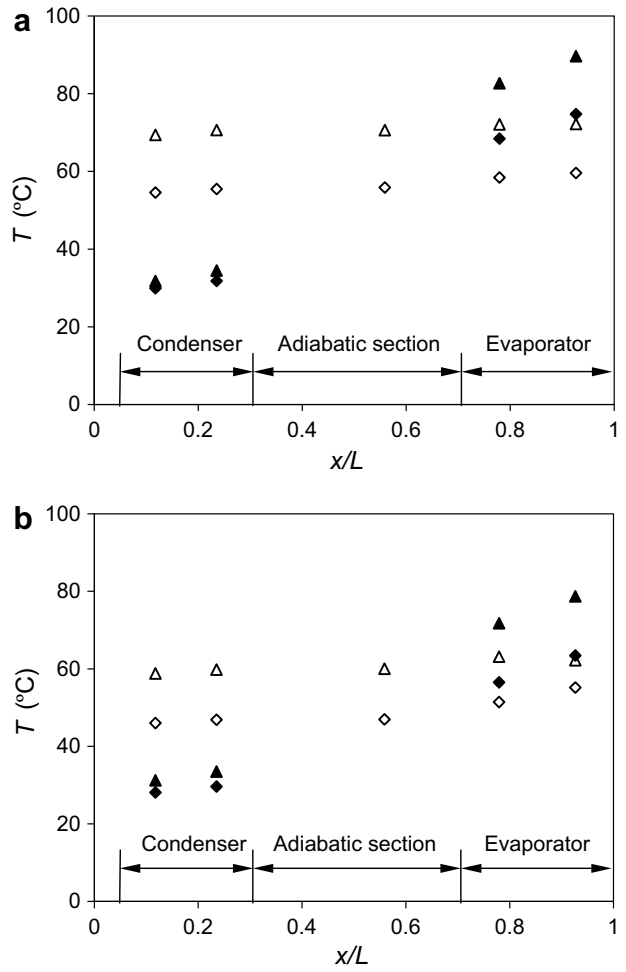

Fig. 4. Typical axial temperature distributions in the wall (solid symbols) and the core region (open symbols) of the cylindrical heat pipe at (a) 2000 rpm, and ◆◇ 0.34 kW, ▲ △ 0.51 kW; and at (b) 4000 rpm, and ◆◇ 0.31 kW, ▲△ 0.48 kW.

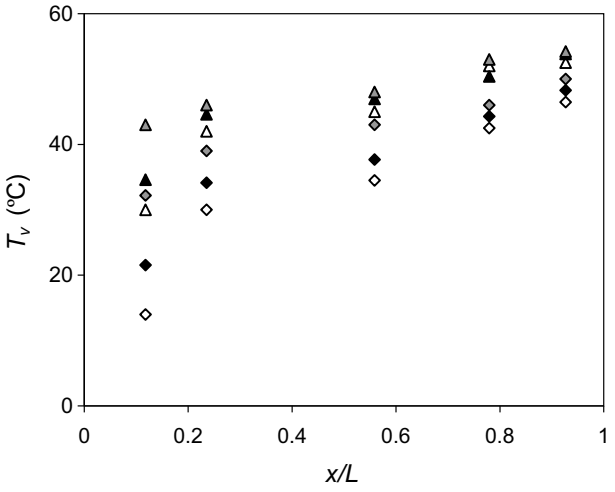

Fig. 5. Change in the core temperature distribution for the tapered heat pipe at 2000 rpm for heat transfer rates of ◇ 0.25 kW, △ 0.48 kW when the cooling water inlet temperature $T_{c,i} = 12.8$ °C; and for ◆ 0.25 kW, ▲ 0.48 kW when $T_{c,i} = 19.2$ °C; and for ◆ 0.25 kW, ▲ 0.48 kW when $T_{c,i} = 28.8$ °C.

shown in numerical simulations of the vapour flow at higher rotational speeds or lower heat fluxes [7,17].

There was also a significant temperature decrease in the core region of the condenser section for the tapered heat pipe that was not as evident for the cylindrical heat pipe. This was particularly true at low heat fluxes suggesting that the non-uniform temperature in the condenser region may be due to the presence of non-condensable gases that tend to accumulate in the region near the end of the condenser [18]. The source of the non-condensable gases is not clear, but could likely be related to the installation of the internal instrumentation. The temperature distribution in the tapered heat pipe was measured for different inlet cooling water temperatures and the results for 2000 rpm are shown in Fig. 5. It is clear that the temperature distribution in the core region became more uniform as the core temperature increased due to either an increase in the inlet water temperature or an increase in the heat transfer rate through the heat pipe. This is consistent with the interpretation that this is caused by non-condensable gases. The saturation pressure changed by a factor of almost 20 with the increase in operating temperature considered here. The temperature of the non-condensable gases tended to follow the condenser wall temperature and only changed by about 5% in absolute terms. Thus the change in the volume of the non-condensable gases was largely determined by the change in the pressure of the non-condensable gases. The more uniform temperature distributions in the condenser section of the cylindrical heat pipe suggest that the effect of non-condensable gases was smaller in this case.

Thus, the results suggest that the wall temperature measured in the condenser further away from the end cap ($T_{wc,2}$ in Fig. 2) was a better measure of the wall temperature in the active region of the condenser and was used to represent the wall temperature of the condenser section. Since the local heat flux at the evaporator is not known, it was necessary to select a representative wall temperature for the evaporator section. In the case where the temperature distribution along the wall is linear and the heat transfer is conduction, the average temperature would be appropriate. In the case of natural convection where the heat transfer coefficient would vary with the temperature difference, it was appropriate at least to first order. The two thermistors along the evaporator wall are located so that they yield the average of the temperature distribution, which was corroborated by the thermal camera images. Therefore, the overall heat transfer performance of the heat pipes was characterized using the overall thermal resistance R given by

$$R = \frac{T_{we} - T_{wc}}{Q}, \tag{2}$$

where $T_{we} = (T_{we,1} + T_{we,2})/2$ and $T_{wc} = T_{wc,2}$. Similarly, the temperature measured in the core region of the adiabatic section (T_{va} in Fig. 2) was thought to be the best

measure of the saturation temperature. In this case, the heat transfer performance in the evaporator and condenser sections were characterized by the thermal resistances R_e and R_c given by

$$R_e = \frac{T_{we} - T_{va}}{Q}, \tag{3}$$

and

$$R_c = \frac{T_{va} - T_{wc}}{Q}. \tag{4}$$

The relative uncertainties in the computed thermal resistances varied from ±22% to ±8% at the 95% confidence interval as the heat transfer rates through the heat pipe increased.

The changes in the overall thermal resistance of the two heat pipes and the resistances of the individual sections with heat transfer rate are shown in Fig. 6. The thermal resistances of the evaporator and condenser sections were similar in the tapered heat pipe at both speeds indicating both sections were important in determining the overall performance of the tapered heat pipe. The thermal resistance of the condenser section in the cylindrical heat pipe, however, was significantly larger than the evaporator section and thus played a larger role in determining the performance of this heat pipe, as expected.

The thermal resistance of the condenser section in both heat pipes decreased with an increase in rotational speed due to the increase of the driving force within the liquid layer which should reduce the liquid film thickness in the condenser section [8–10]. The thermal resistance of the condenser section also decreased significantly with heat flux. Part of this was likely due to the presence of the non-condensable gas. The increase in operating temperature of the heat pipe with heat flux tends to decrease the volume of non-condensable gases, as noted above. The thermal resistance of the evaporator section in both heat pipes decreases with rotational speed, consistent with a natural convection mechanism that would be enhanced with an increase in the rotational speed. The results do not seem to be consistent with conduction across the liquid layer because the increase in speed should redistribute the liquid film towards the evaporator section [8], increasing the liquid layer thickness and the resistance to conduction heat transfer. The thermal resistance of the evaporator also decreased with the heat transfer rate, again consistent with a natural convection mechanism that would be enhanced with an increase in the temperature difference across the liquid layer.

The measurements were compared to predictions from an existing model for non-stepped rotating heat pipes proposed by Song et al. [8]. In this model, the equations for the liquid flow and heat transfer in the condenser, the adiabatic section and the evaporator are coupled and solved as a one-domain problem for the overall heat transfer. The condenser is modeled using a modified Nusselt-type filmwise condensation approach, while the evaporator is modeled using a film evaporation that considered both conduction

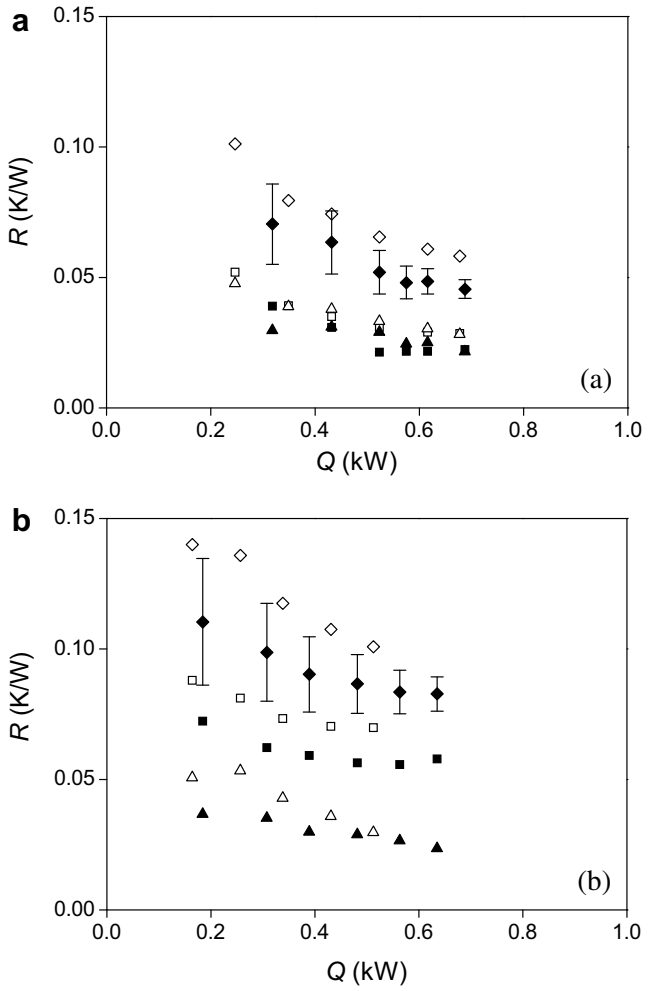

Fig. 6. Change in ◇◆ the overall thermal resistance R and the thermal resistances of □■ the condenser section R_c and △▲ the evaporator section R_e with heat flux determined from measurements at 2000 rpm (open symbols) and 4000 rpm (solid symbols) for (a) the tapered heat pipe and (b) the cylindrical heat pipe.

and acceleration induced natural convection within the liquid film by incorporating a correlation for natural convection in liquid pools under acceleration [14]. Calculations were also performed using a model proposed by Li et al. [6] that only considered conduction across the film in the evaporator. Both models were also modified to incorporate a simplified model for the effect of non-condensable gases in the condenser section [18]. In particular, the condenser section was modeled as consisting of an inactive region near the end cap in thermal equilibrium with the heat sink, and an active region that contained only saturated vapour. It is assumed that the inactive region consists of a mixture of water vapour and all the non-condensable gases. The total pressure in this region is assumed to be the same as the saturation pressure in the active region of the heat pipe by neglecting the pressure drop from end to end, and the partial pressure of vapour is determined by the local temperature. Thus, the pressure of the non-condensable gases itself is estimated as the difference between the total pres-

sure and the partial pressure of the vapour in the inactive region. Each of these was determined from the core temperature in the condenser using the embedded thermistors located at both ends of the condenser section.

The boundary between the active and inactive regions was modeled as a flat front at a position

$$L_{c,in} = \frac{m_g R_g T_{g,in}}{(p_{v,ac} - p_{v,in}) A_v}, \quad (5)$$

from the end of the heat pipe. Here, $T_{g,in}$ is the temperature of the non-condensable gases that was estimated using the cooling water inlet temperature, while $p_{v,ac}$ and $p_{v,in}$ are the pressure of the vapour in the active and inactive regions. The non-condensable gas was modeled as air in this study.

The thermal resistances from the measurements are compared to the predictions from Song et al.'s model for both heat pipes in Figs. 7 and 8. The predictions for the case with no non-condensable gases and two cases with 3×10^{-7} and 6×10^{-7} g of non-condensable gases are shown in the figures. The predicted evaporator thermal resistance was relatively independent of the amount of non-condensable gases, and in good agreement with the measurements for both heat pipes with a difference less than approximately 10%. This was much better than the results when conduction heat transfer alone was considered in the evaporator. In those cases, the thermal resistance of the evaporator was up to three times larger than the measurements, particularly for the tapered heat pipe that contained a larger amount of working fluid. The models predicted that the excess working fluid tends to pool in the evaporator, significantly increasing the thermal resistance when conduction alone is considered.

The thermal resistances of the condenser section predicted using Li et al.'s model were very similar to those using Song et al.'s model shown in the figures. The predictions of the condenser thermal resistance that did not con-

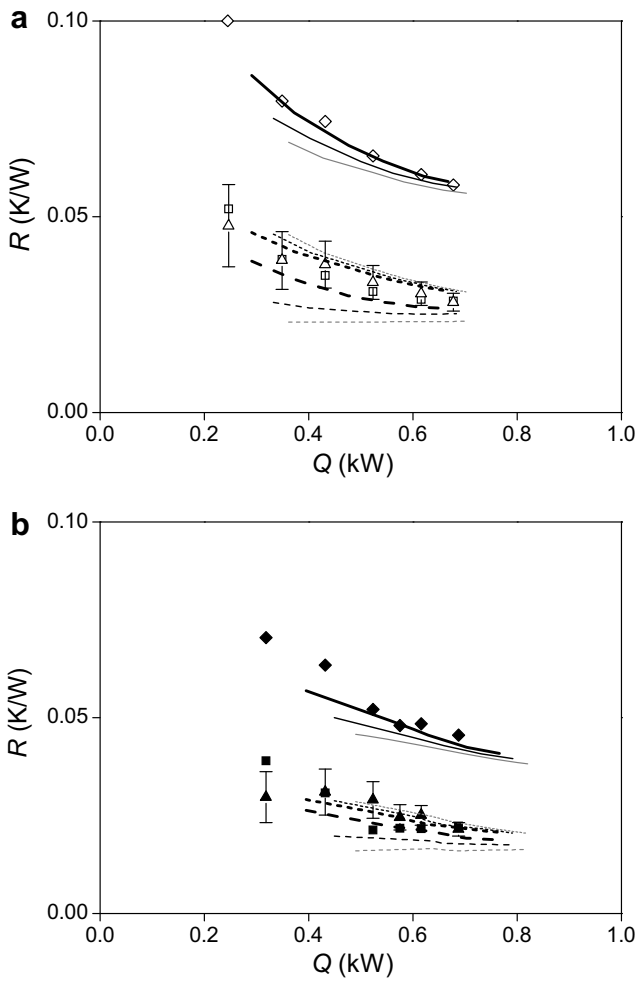

Fig. 7. Change in ◇◆R, □■ R_c, and △▲R_e with heat flux for the tapered heat pipe determined from measurements at (a) 2000 rpm (open symbols) and (b) 4000 rpm (solid symbols); and predictions from Song et al.'s model [8] for ———, ———, ——— R, — — —, — — —, — — — R_c, and – – – –, – – – –, – – – – R_e for the cases of 0, 3×10^{-7}, and 6×10^{-7} g of non-condensable gases, respectively.

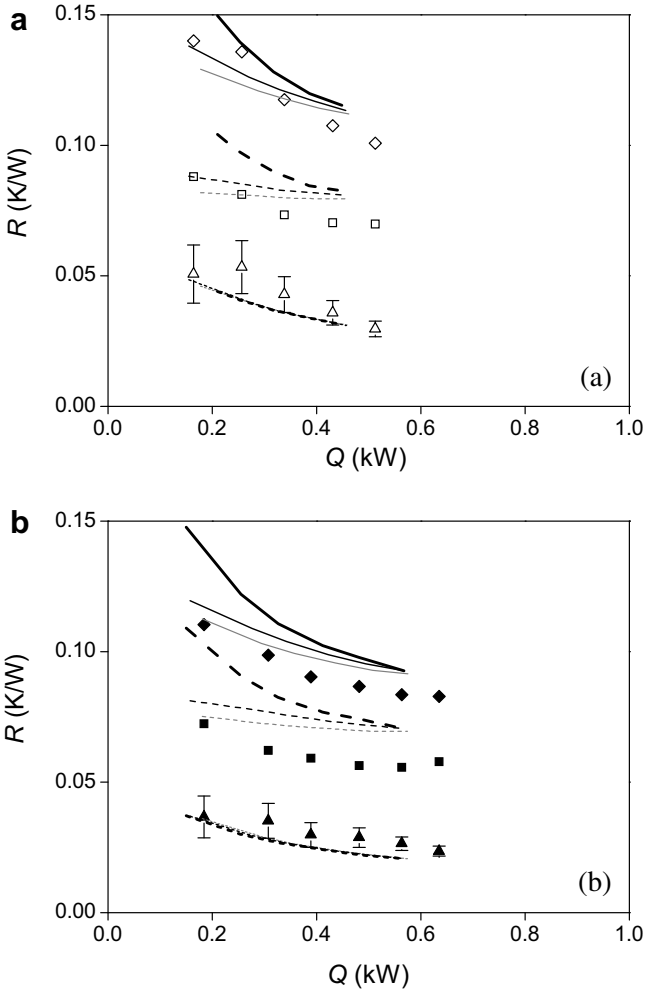

Fig. 8. Change in ◇◆R, □■ R_c, and △▲R_e with heat flux for the cylindrical heat pipe determined from measurements at (a) 2000 rpm (open symbols) and (b) 4000 rpm (solid symbols); and predictions from Song et al.'s model [8] for ———, ———, ——— R, — — —, — — —, — — — R_c, and – – – –, – – – –, – – – – R_e for the cases of 0, 3×10^{-7}, and 6×10^{-7} g of non-condensable gases respectively.

sider the effect of the non-condensable gases were relatively independent of the heat flux, unlike the measurements. The predicted condenser thermal resistance decreased with heat flux when the non-condensable gases were included in the model. The change in the thermal resistance with heat flux increased with the amount of non-condensable gases, indicating that the non-linearity in the thermal resistance may be an indication of the amount of non-condensable gases present in the heat pipe. A more complex model for the non-condensable gas distribution would likely be required, though, to properly predict the effect of the gases at low heat fluxes. The amount of non-condensable gases had less effect on the predicted thermal resistance at larger heat fluxes. The predictions for the condenser thermal resistance for the tapered heat pipe were in reasonable agreement with the measurements. The model, however, overestimated the measurements for the cylindrical heat pipe even at high heat fluxes, the cause of which is not clear.

The heat transfer in the evaporator sections of the two heat pipes for all cases in terms of the Nusselt number and Rayleigh number for the liquid film is shown in Fig. 9. The liquid film thickness used to compute the Nu_δ and Ra_δ here is the average value in the evaporator section predicted from the model. The results agree with the correlation $Nu_\delta = 0.133 Ra_\delta^{0.375}$ for natural convection in liquid pools under acceleration [14] when $Ra_\delta \geqslant 400$. When $Ra_\delta \leqslant 400$, the computed Nusselt number was approximately 1, consistent with conduction heat transfer across the liquid layer. The transition Rayleigh number of approximately 400 is much lower than the conventional criterion of $Ra_\delta > 1000$ for the onset of natural convection [19]. This is, however, consistent with the observations of Zhang and Chao [20] who found that Benard-type natural convection occurred at lower Rayleigh numbers in the presence of film evaporation. Zhang and Chao [20] proposed a modified Rayleigh number to include the contribution of film evaporation. This modified Rayleigh number with the gravitational acceleration g replaced with the centrifugal acceleration $\omega^2 r$ is given by

$$Ra_\delta^* = \frac{\rho_l \omega^2 r \cos\alpha \beta \Delta T \delta^3}{\mu_l \alpha_l}\left(1 + \frac{h_{\mathrm{hg}} \dot{V} \delta}{c_{p_l} \alpha_l \Delta T}\right) = Ra_\delta \left(1 + \frac{h_{\mathrm{hg}} \dot{V} \delta}{c_{p_l} \alpha_l \Delta T}\right). \quad (6)$$

The first term is the conventional Rayleigh number, while the second term accounts for the effect of film evaporation. The estimate of Ra_δ^* at the transition in the Nusselt number for the evaporator section here was 800–1100, in agreement with the criterion for the onset of natural convection without film evaporation [19].

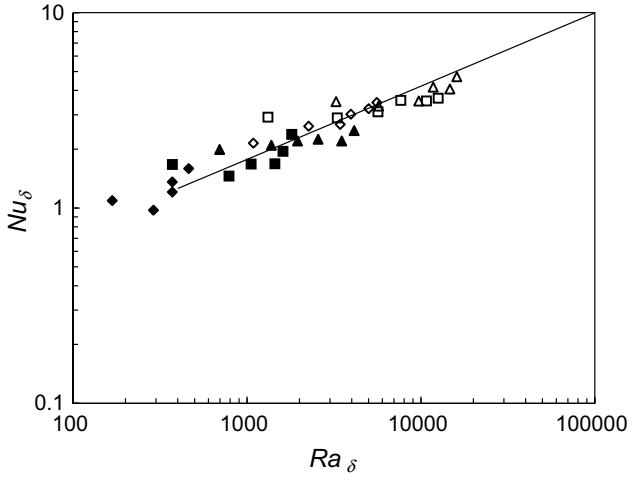

Fig. 9. Change in Nu_δ with Ra_δ for the liquid film in the evaporator of the tapered heat pipe (open symbols) and the cylindrical heat pipe (solid symbols) for rotational speeds of ◇◆ 2000 rpm, □■ 3000 rpm, △▲ 4000 rpm and —— the correlation for natural convection heat transfer proposed by Körner [14].

4. Conclusions

Experiments were performed to investigate the heat transfer in the evaporator section of non-stepped rotating heat pipes at moderate rotational speeds. The measurements show that the thermal resistance of the evaporator section decreased with an increase in either the rotational speed and or the heat flux, consistent with a natural convection heat transfer mechanism within the liquid layer. The thermal resistance of the evaporator section was lower than that of the condenser for the cylindrical heat pipe, but nearly the same as the condenser section in the tapered heat pipe. The experimental results for the heat transfer in the evaporator were reasonably predicted using the model that considered the effects of natural convection in the evaporator [8], but deviated from the model predictions that considered conduction alone [6]. The heat transfer measurements in the evaporator were in general agreement with the correlation for natural convection under acceleration developed by Körner [14]. The agreement between the test data and the correlation extended to liquid film Rayleigh numbers as low as 400, indicating natural convection occurred at these low Rayleigh numbers in the presence of film evaporation. The transitional Rayleigh number was evaluated using a modified Rayleigh number for film evaporation applications proposed by Zhang and Chao [20]. The modified Rayleigh number was approximately 10^3 when the centrifugal acceleration was used in place of the gravitation acceleration in the proposed expression.

Acknowledgement

The support of the Natural Sciences and Engineering Research Council (NSERC) of Canada and Pratt and Whitney, Canada is gratefully acknowledged.

References

[1] V.H. Gray, The rotating heat pipe – A wickless hollow shaft for transferring high heat fluxes, ASME No. 69-HT-19, 1969.

[2] G. Gutierrez, T.C. Jen, Performance of an axially rotating heat pipe in drilling applications, 9th Latin American Congress in Heat and Mass Transfer, Puerto Rico, 2002.
[3] R. Ponnappan, Q. He, J.E. Leland, Test results of a high speed rotating heat pipe, AIAA Paper No. 97-2543, 1997.
[4] G.P. Peterson, An Introduction to Heat Pipes, John Wiley & Sons, Inc., New York, 1994.
[5] L.L. Vasiliev, V.V. Khrolenok, Heat transfer in rotating heat pipes, Proceedings of the 7th International Heat Pipe Conference, USSR, 1990, pp. 285–294.
[6] H.M. Li, C.Y. Liu, M. Damodaran, Analytical study of the flow and heat transfer in a rotating heat pipe, Heat Recov. Syst. CHP 63 (1993) 115–122.
[7] C. Harley, A. Faghri, Two-dimensional rotating heat pipe analysis, J. Heat Transfer 117 (1995) 202–208.
[8] F. Song, D. Ewing, C.Y. Ching, Fluid flow and heat transfer model for high-speed rotating heat pipes, Int. J. Heat Mass Transfer 46 (2003) 4393–4401.
[9] T.C. Daniels, F.K. Al-Jumaily, Investigation of the factors affecting the performance of a rotating heat pipe, Int. J. Heat Mass Transfer 18 (1975) 961–973.
[10] P.J. Marto, Performance characteristics of rotating wickless heat pipes, Proceedings of the 2nd International Heat Pipe Conference, Bologna, Italy, 1976, pp. 281–291.
[11] W. Nakayama, Y. Ohtsuka, H. Itoh, T. Yoshikawa, Optimum Charge of Working Fluids in Horizontal Rotating Heat Pipes, in: D.E. Metzger, N.H. Afgan (Eds.), Heat and Mass Transfer in Rotating Machinery, Hemisphere, Washington, D.C., 1984, pp. 633–644.
[12] R.L. Judd, H. Merte Jr., Evaluation of nucleate boiling heat flux predictions at varying levels of subcooling and acceleration, Int. J. Heat Mass Transfer 15 (1972) 1075–1096.
[13] P.J. Marto, Rotating Heat Pipes, in: D.E. Metzger, N.H. Afgan (Eds.), Heat and Mass Transfer in Rotating Machinery, Hemisphere, Washington, D.C, 1984, pp. 609–632.
[14] W. Körner, Influence of higher acceleration on heat flow in boiling, Chemie Ing. Techn. 42 (1970) 409–414, in German.
[15] F. Song, D. Ewing, C.Y. Ching, Experimental investigation on the heat transfer characteristics of axial rotating heat pipes, Int. J. Heat Mass Transfer 47 (2004) 4721–4731.
[16] H.W. Coleman, W.G. Steele, Experimentation and Uncertainty Analysis for Engineers, John Wiley & Sons, New York, 1999.
[17] A. Faghri, S. Gogineni, S. Thomas, Vapor flow analysis of an axially rotating heat pipe, Int. J. Heat Mass Transfer 36 (1993) 2293–2303.
[18] S.W. Chi, Heat Pipe Theory and Practice, Hemisphere, 1976.
[19] A. Bejan, Convection Heat Transfer, John Willy & Sons, 1984.
[20] N.L. Zhang, D.F. Chao, Mechanisms of convection instability in thin liquid layers induced by evaporation, Int. Commun. Heat Mass Transfer 26 (1999) 1069–1080.